Osteoarthritis and Cartilage 22 (2014) 1410–1418

Osteoarthritis and Cartilage

OARSI OSTEOARTHRITIS RESEARCH SOCIETY INTERNATIONAL

In vitro glycation of articular cartilage alters the biomechanical response of chondrocytes in a depth-dependent manner

J.M. Fick*, M.R.J. Huttu, M.J. Lammi, R.K. Korhonen

Department of Applied Physics, University of Eastern Finland, Kuopio FI-70211, Finland

ARTICLE INFO

Article history:
Received 13 February 2014
Accepted 18 July 2014

Keywords:
Articular cartilage
Aging
Cross-linking
Ribose
Chondrocyte deformation

SUMMARY

Objective: To determine if increasing cartilage cross-links through *in vitro* glycation of cartilage explants can alter the biomechanical response of chondrocytes to compressive deformation.
Method: Bovine osteochondral explants were either incubated with cell culture solution supplemented with ($n = 7$) or without ($n = 7$) ribose for 42 h in order to induce glycation. Deformation-induced changes in cell volume, dimensions and local tissue strains were determined through confocal laser scanning microscopy (CLSM) and the use of a custom built micro-compression device. Osteochondral explants were also utilized to demonstrate changes in depth-wise tissue properties, biomechanical tissue properties and cross-links such as pentosidine (Pent), hydroxylysyl pyridinoline (HP) and lysyl pyridinoline (LP).
Results: The ribose treated osteochondral samples experienced reduced cell volume deformation in the upper tissue zone by ~8% ($P = 0.005$), as compared the control samples, through restricting cell expansion. In the deeper tissue zone, cell volume deformation was increased by ~12% ($P < 0.001$) via the transmission of mechanical signals further into the tissue depth. Biomechanical testing of the ribose treated osteochondral samples demonstrated an increase in the equilibrium and dynamic strain dependent moduli ($P < 0.001$ and $P = 0.008$, respectively). The biochemical analysis revealed an increase in Pent cross-links ($P < 0.001$). Depth-wise tissue property analyses revealed increased levels of carbohydrate content, greater levels of fixed charge density and an increased carbohydrate to protein ratio from 6 to 16%, 55–100% and 72–79% of the normalized tissue thickness (from the surface), respectively, in the ribose-treated group ($P < 0.05$).
Conclusion: In vitro glycation alters the biomechanical response of chondrocytes in cartilage differently in upper and deeper zones, offering possible insights into how aging could alter cell deformation behavior in cartilage.

Introduction

Like other connective tissues within the body, articular cartilage (AC) is susceptible to age-related changes. Nearly half of all persons over 65 years suffer from osteoarthritis (OA) in the USA[1]. Hence, it is not surprising that aging is a major risk factor in the development of OA[2]. The traditional explanation offered is that mechanical loading of AC over its life cumulatively affects it, resulting in "wear and tear" and eventual breakdown[3] of this joint tissue. However, recent research is suggesting that this is not the case[3–7].

Researchers are now focusing on understanding how cells respond to and convert mechanical signals into biomolecules aimed at tissue maintenance/remodelling[6–8]. Because the biological responses (i.e., cell metabolism) of chondrocytes (cells) in AC are related to the mechanical signals that they experience[6–9] understanding how mechanical signals can drive cell responses is important in understanding the aging process and how it can trigger the development of OA. Cartilage research has so far demonstrated that aging increases the stiffness of both the ECM (the extracellular matrix of AC)[10–15] and chondrocytes[16,17], decreases the viscoelastic properties of the local cellular matrix (termed the pericellular matrix or PCM)[17], modifies cellular metabolism and metabolic pathways[3–7,11,18–20] and ultimately increases the tissue's susceptibility to fracture[13–15]. Age-related deterioration of AC appears to be a problem that involves both tissue and cellular-scale changes. Thus, understanding how cells respond to

* Address correspondence and reprint requests to: J.M. Fick, Department of Applied Physics, University of Eastern Finland, Kuopio FI-70211, Finland. Tel: 358-50-5914016.
E-mail address: jfickbiomaterials@yahoo.com (J.M. Fick).

http://dx.doi.org/10.1016/j.joca.2014.07.020
1063-4584/

deformation within aged AC is important in identifying mechano-biological differences due to tissue aging.

It is well documented that advanced glycation end products (AGEs) accumulate within the ECM[12–15,17–20] during aging, resulting in increased levels of cross-linking, particularly in long-lived proteins, such as collagens. Treatment of AC with sugars, such as ribose[11,14,15,19,20] and threose[13,19–21], have been used to mimic the aging process to demonstrate that cross-linking can alter the mechanical properties of AC and possibly cause tissue dysfunction, degeneration and/or OA[3–9,13–15]. Although these treatments provide a faster means of inducing *in vitro* glycation, they may not completely mimic the age-related non-enzymatic products that form *in vivo*[22–25].

Other studies have investigated the biomechanical response of chondrocytes and/or their PCM in AC by utilizing unconfined compression[26,27] and indentation techniques[28–30]combined with confocal microscopy or by modeling the stress/strain fields within AC[31–33]. These studies have provided a better understanding of how the ECM/PCM can contribute towards modifying the response of chondrocytes to compression. However, it is not known how or if inducing cross-links within AC can alter the response of chondrocytes to deformation in cartilage.

This study's aim is to investigate how chondrocytes in normal and artificially cross-linked osteochondral explants mechanically respond to deformation. In order to achieve this, ribose was used to induce cross-linking within AC. Chondrocyte deformation was investigated through the use of a custom built micro-compression device and confocal laser scanning microscopy (CLSM). Osteochondral explants were also utilized to demonstrate changes in biomechanical tissue properties. Biochemical analysis for cross-links such as pentosidine (Pent), hydroxylysyl pyridinoline (HP) and lysyl pyridinoline (LP) were performed through high-performance liquid chromatography (HPLC)[21]. This enabled us to chemically confirm changes in the levels of cross-links between untreated (control) and ribose-treated (treated) groups. Digital densitometry (DD), Fourier Transform infrared spectroscopic imaging (FTIRI) and polarized light microscopy (PLM) were also performed to investigate depth-wise structure and composition of the tissues.

Methods

A brief description of the materials and methods is given here. More details are listed in the Supplemental Material.

Sample preparation

Surface intact osteochondral plugs (ø = 31 mm) were harvested from the lateral aspect of the distal pole of patellae obtained from seven separate bovine animals. The patellae were obtained from a local abattoir (Atria Oyj, Kuopio, Finland) and the age of the animals at the time of slaughter was 18 ± 1 months. The total number of animals utilized in this study was based on previous glycation research that demonstrated statistical differences from utilizing patellar cartilage from a total of seven bovine animals[21]. Each plug had two osteochondral samples removed (ø = 8 mm; Fig. 1) and these were randomly placed into a control or treated group ($n = 7$/group). Samples were then incubated (for 42 h) in cell culture medium with 30 mM of ribose supplemented in the medium (treated group) or without (control group) ribose supplementation. The remnant tissue portions (Fig. 1) were carried through the identical incubation process described for the osteochondral samples. After incubation, each osteochondral sample had a smaller osteochondral plug (ø = 2.9 mm) removed for biomechanical testing (Fig. 1). The remaining osteochondral samples were cut into

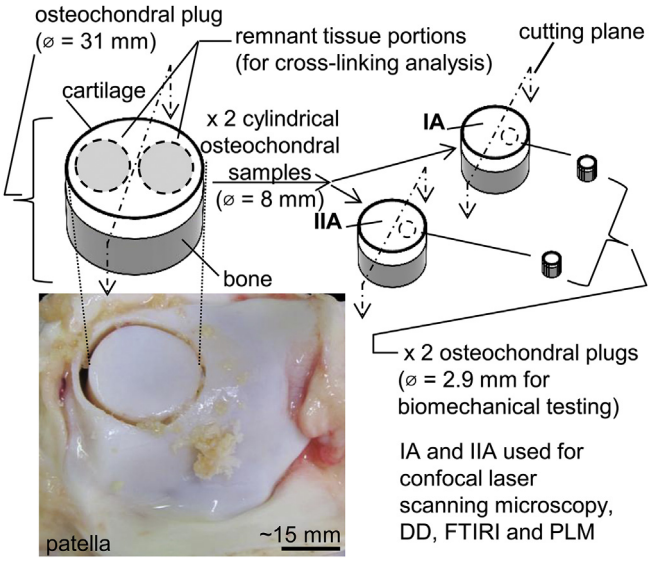

Fig. 1. Schematic diagram illustrating the sample preparation steps used for the cartilage samples.

hemi-cylindrical samples and were used for cell deformation experiments (Fig. 1) and then subsequent analysis for depth-wise tissue structure and composition. The cartilage from the remnant tissue portions was removed from underlying bone; had their wet weights determined and analyzed biochemically for cross-links.

Cell deformation experiments

The hemi-cylindrical samples were stained for 30 min with both calcein-AM (5 μM, Invitrogen, Eugene, OR, USA) and propidium iodide (60 μM, Sigma, Ronkonkoma, NY, USA) for live and dead cells, respectively. Following staining, samples were positioned cut tissue side down (with the exposed bone surface against the loading bar) into a sample bath of a custom built stainless steel micro-compression device [Fig. 2(a)-i]. The samples were kept hydrated by filling the chamber with Dulbecco's Modified Eagle Medium (DMEM) (1 g/l low glucose, Gibco, Eugene, OR, USA) throughout testing.

An inverted CLSM Zeiss LSM 700 (Zeiss Axio Observer .Z1, Carl Zeiss, Oberkochen, Germany) was used for microscopic imaging [Fig. 2(a)-ii]. To perform cell deformation experiments, the micro-compression device was fitted into the microscope stage [Fig. 2(a)-ii]. Initial contact between the articular surface and the side of the sample bath was visually confirmed through the use of a 10× magnification objective. Tissue thickness was then estimated by measuring the distance between the surface to cartilage–bone interface through the confocal microscope computer software (Zen 2009, Carl Zeiss, Germany). An undeformed image stack of the entire sample (from the tissue surface to cartilage–bone interface) and higher magnification image stacks of chondrocytes within the "upper", "middle" and "deep" tissue zones were taken prior to deformation (using a ×10 magnification objective and an ×40 magnification oil immersion objective, respectively; Fig. 2(b), (c)). Each sample was then deformed by 15% and the tissue was allowed to relax for 45 min[21]. After tissue deformation, image stacks of chondrocytes within the "upper", "middle" and "deep" tissue zones and fully deformed tissue thickness image stacks were obtained [see Fig. 2(b), (c)]. For the purposes of this study, the upper zone was defined to be from the cartilage surface up to 15% depth from the surface, the middle zone from 15% to 41% depth from the tissue

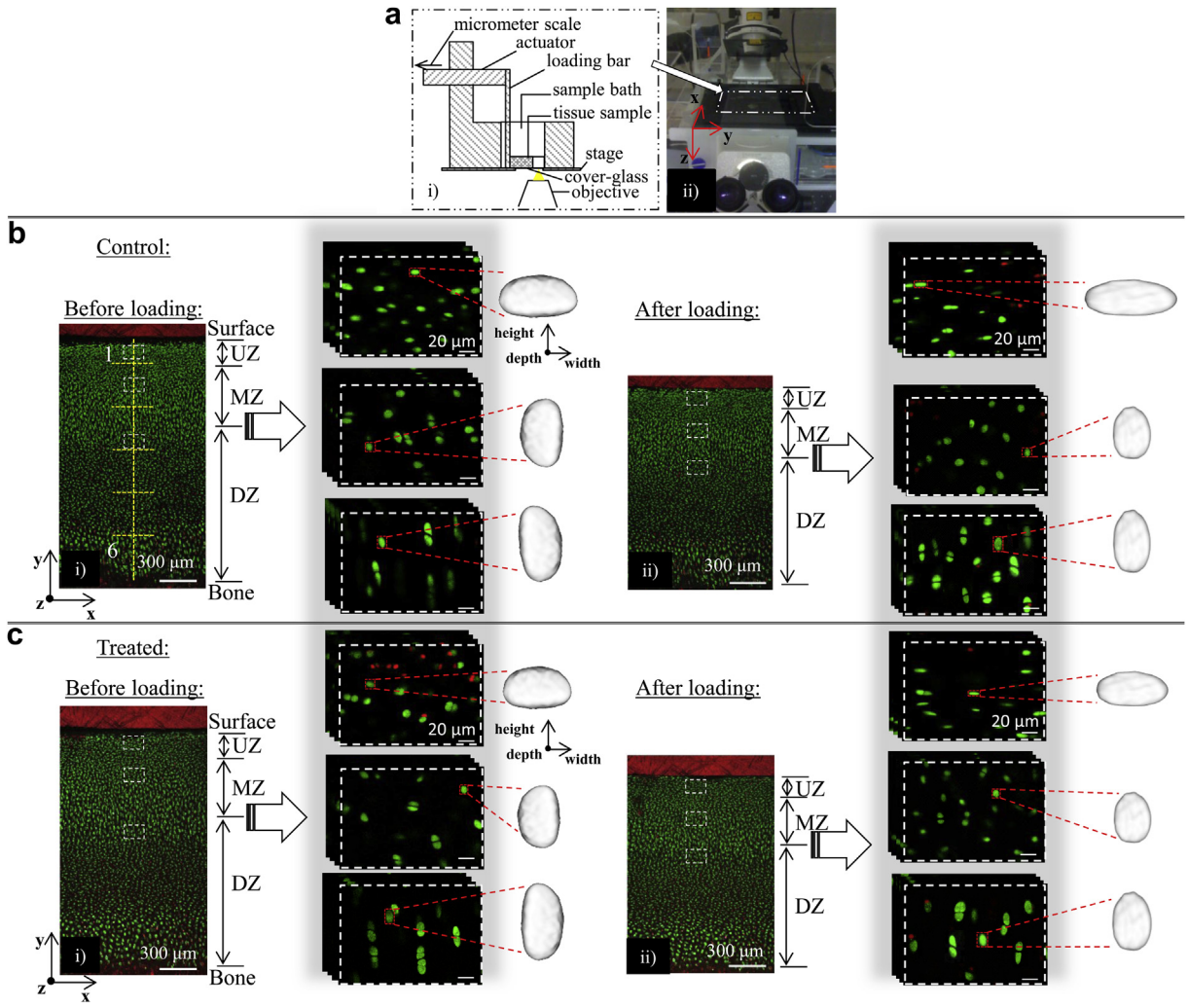

Fig. 2. A schematic illustrating the steps utilized for CLSM and subsequent analysis. a) cross-section schematic illustrating the micro-compression device (i) used for the chondrocyte deformation measurements and the orientation of it positioned into the confocal laser scanning microscope (ii). The micro-compression device is positioned into the confocal microscope device as outlined by the dashed-line box; b) CLSM images (×10 low magnification and ×40 higher magnification images) and adjacent idealized 3D reconstructions obtained from cells from each inspected zone within the control tissue before (i) and after compression (ii). An idealized 3D cell reconstruction was selected to demonstrate shape changes across each of the tissue zones before and after loading; c) CLSM images (×10 low magnification and ×40 higher magnification images) and 3D-cell reconstructions obtained from each inspected zone within the treated tissue before (i) and after compression (ii). Live cells are stained green (red stained cells are dead cells). Cell height, width and depth axis indicates cell dimensions. The superimposed yellow-dashed lines depict regions 1 through 6 which were used for determining local strains in each tissue.

surface and the deep zone from 41% to 100% depth from the tissue surface[34]. Cell volume, height, width and depth as well as local tissue strains were then analyzed.

The ×40 magnification image stacks were imported into ImageJ (National Institute of Health, USA). For the cell volume reconstructions, only viable (bright green labeled cells) cells were selected and individual cell image stacks that fully encapsulated each selected cell were cropped from the original image stack. Eight to ten viable cells from each of the upper, middle and deep zones within each sample were individually selected and saved to determine cell volume and dimensions across each group cohort [Fig. 2(b), (c)]. Please refer to Supplemental Table 1 for cell numbers determined across each tissue group. 3-D images of these cells were generated by the Visualization Toolkit 5.2.0 (Kitware Inc.; see the cell reconstructions in Fig. 2(b), (c)) and cell volumes were calculated by an analysis script programmed with Python. A threshold of 40% of the maximum cell fluorescence intensity[35] was used in the volume calculation. Using Matlab R2007b (Mathworks Inc., USA)[29], height and width measurements of cells were defined along the major and minor cells axis. These major and minor directions were opposite in the upper and deep zones [see Fig. 2(b), (c)]. Cell depth directions (z-direction from the image stacks) were also determined (Using Matlab) by measuring the perpendicular distance between the cell surfaces at the point where the major and minor cell axis intersected in each cell. In order to investigate the response of chondrocytes to deformation across each tissue group, deformation-induced percent changes in cell volumes, heights, widths and depths were calculated from the original cell volume and dimensional data ([(after − before)/before] ×100) for each tissue zone.

Local axial and transverse cartilage strains were determined by using the ×10 magnification images. Both the before and after deformation images from each tissue were divided into six equally spaced regions, depth-wise, from the surface to the cartilage–bone

interface across the central region of each image [Fig. 2(b)]. Three cell pairs were identified from each before and after deformation image in each of the six regions from each sample ($n = 21$ cell pairs/region within each group). Vertical and horizontal distances between these cell pairs were measured in the before and after deformation images to determine local axial ([(before − after)/before] ×100) and transverse strains ([(after − before)/before] ×100) in each tissue region.

Biomechanical testing and biochemical analysis

Biomechanical testing was performed to quantify changes in the equilibrium and dynamic moduli of the samples as a result of ribose treatment ($n = 7$ samples/group). Full thickness tissue samples were analyzed for levels of HP, LP and Pent with an HPLC ($n = 7$ samples/group).

Depth-wise analysis of tissue composition and structure

Optical density (from Safranin-O staining using DD)[36], carbohydrate content (from the carbohydrate region of the FTIRI spectrum between 900 and 1200 cm^{-1})[37], protein content (from the Amide I and II regions of the FTIRI spectrum between 1480 and 1700 cm^{-1})[37] and collagen orientation angle (using PLM[38]) were measured for both groups in a depth-wise manner from a total of 21 sections from each group for each method. Optical density can be used as an estimate of fixed charge density and the carbohydrate content determined through the use of FTIRI can provide an overall indication of the levels of glycation[39] and the relative abundance expressed in terms of a carbohydrate to protein ratio has been indicated to reflect the region in the spectrum over which glycated proteins and/or AGE-like moieties exist[37].

Statistical methods

All data was pooled according to the experimental test, tissue group, zone and whether the cells came from deformed tissue (only applicable for the cell deformation experiments). The data was then assessed for normality by using Shapiro–Wilk statistical tests ($P < 0.05$). Based on this analysis, non-parametric statistical tests were utilized for cell volume and dimensional data. Parametric statistical tests were used for the local strain, biomechanical, biochemical and depth-wise tissue data. All statistical analyses were performed using IBM SPSS Statistics 21.0 (IBM Corp, Armonk, NY, USA). Data was expressed as median or mean (accordingly) with 95% confidence intervals (CI).

Two-tailed, independent sample median tests were used to determine if the cell volumes and cell heights, widths and depth dimensions were different between the undeformed control and treated groups ($P < 0.05$). Two-tailed, Wilcoxon Signed Rank tests were used to determine differences in cell volumes, heights, widths and depths for each zone from each tissue group (i.e., before vs after deformation; $P < 0.05$). Two-tailed, Mann–Whitney tests to compare independent groups (i.e., control vs treated cell groups from the same zones; $P < 0.05$) were used to determine differences between the deformation-induced percent changes in cell volumes, heights, widths and depths.

For local axial and transverse strain data, biomechanical data (E_{eq}, E_0, E_ε), biochemical data (% water, collagen content, Pent, HP, LP) and data on depth-wise tissue properties (DD, FTIRI and PLM), two-tailed, Student's *t*-tests (due to the aforementioned normality of the data) were utilized to determine differences between these parameters in the control and treated groups ($P < 0.05$).

Results

Deformation-induced cell measurements and local strain analyses

As a result of tissue compression, cell volume increased less in the upper zone of the treated group, as compared to the control group. In the middle zone, cell volume changes were not different between the groups, while a larger cell volume increase in the deep zone of the treated group was observed, as compared to the control group [Fig. 3(a)]. As for the deformation-induced changes in cell dimensions in the treated group relative to the control group, the upper zone of the treated group experienced smaller changes in cell height, width and depth, the middle zone only experienced smaller changes in cell height and depth, and the deep zone experienced larger changes in cell height, width and depth [Fig. 3(b)–(d)].

Local axial and transverse strains gradually decreased from the upper tissue layer down to the cartilage–bone interface in both groups [Fig. 4(a), (b)]. Local axial strain was observed to be smaller in the uppermost tissue layer of the treated group relative to the control group (region 1), while it was found to be greater in the upper-middle region (region 3). No other differences in either local axial strains or in the transverse strains were found between the groups.

See Supplemental Tables 1 and 2 more details of cell volumetric and dimensional data as well as statistical information on the changes in cell parameters due to tissue compression in each tissue zone from each group.

Biomechanical, biochemical, microscopic and spectroscopic analyses

Both the equilibrium and the dynamic strain dependent moduli were greater for the treated group and no differences in the initial dynamic moduli were observed between the groups (Table I). Levels of Pent were greater in the treated group and levels of water, collagen, HP and LP were similar for both groups. In the treated group, increased levels of carbohydrate content, greater levels of fixed charge density (optical density) and an increase in the carbohydrate to protein ratio were found from 6 to 16%, 55–100% and 72–79% of the normalized tissue thickness (from the surface), respectively [Fig. 5(a)–(c)]. The fixed charge density, carbohydrate content and carbohydrate to protein ratio due to ribose treatment were also averaged across the upper, middle and deep tissue zones [Fig. 5(d)–(f)]. Differences in fixed charge density and carbohydrate content were different in all tissue zones [Fig. 5(d), (e)], however the carbohydrate to protein ratio was only different between the control and treated tissue in the deep zone. Depth-wise protein content and collagen orientation angle values were similar between the groups (data not shown).

Discussion

General characteristics of chondrocyte deformation in ribose treated tissues

These results demonstrated that ribose treatment of osteochondral explants decreased the deformation response of chondrocytes to tissue compression in the upper zone while increased the deformation response of chondrocytes in the deep zone. The smaller increase in cell volume change within the upper zone of the treated tissue (relative to the control tissue) was due to a ~9% and ~7% reduction in cell width and depth (respectively). This change was not compensated through a reduction in cell height deformation. Although no differences in cell volume changes were observed in the middle tissue zone between the groups, smaller cell shape changes (height, depth) were observed in the treated group. The

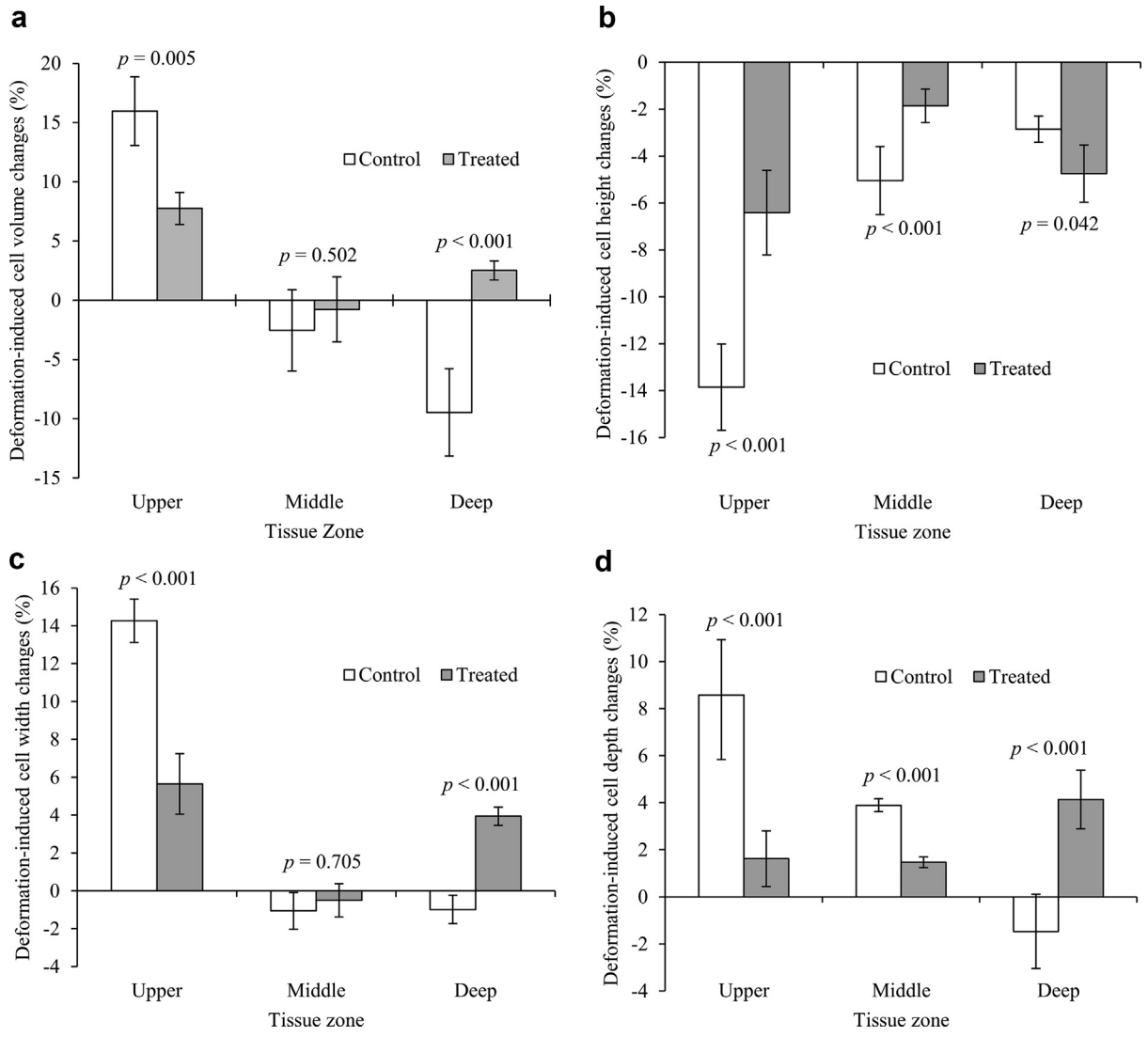

Fig. 3. Median values (±95% CI) of the percent change in cell volume (a), height (b), width (c) and depth (d) due to deformation from the upper, middle and deep tissue zones of the control and treated tissue groups. Statistical differences between the control and treated groups for each tissue zone are denoted by the *P*-values.

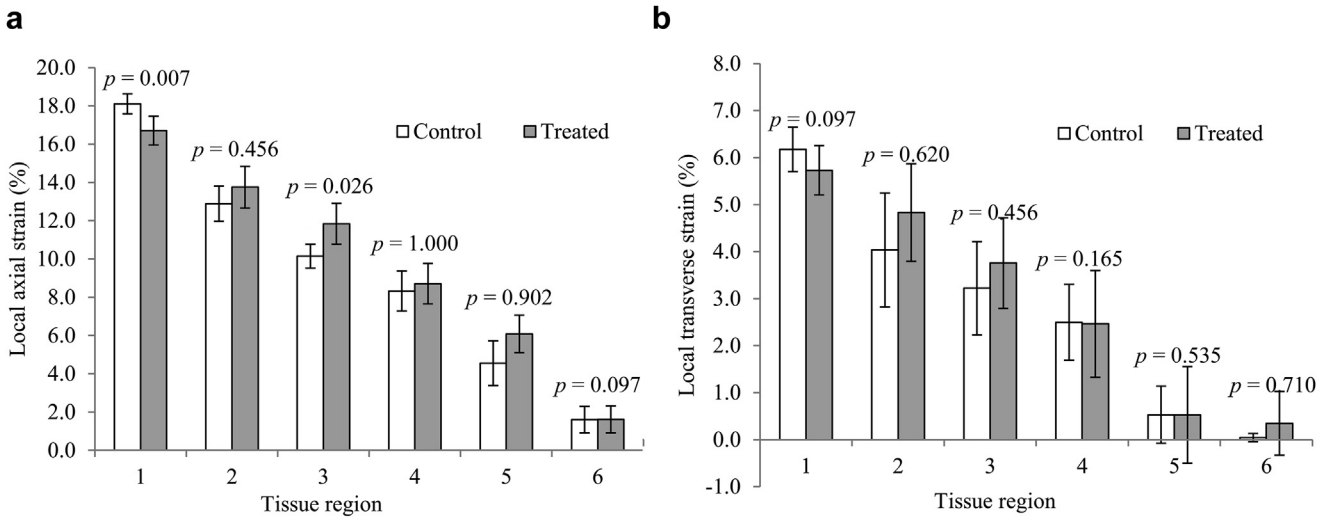

Fig. 4. Mean values (±95% CI) of local axial (a) and transverse strains (b) as determined from six evenly distributed tissue depths from the surface region (1) to the deep tissue region (6) adjacent to the osteochondral junction. Data was obtained across all regions in each sample from each group (see Fig. 2). Statistical differences between groups from each zone are denoted by the *P*-values.

Table I
Equilibrium (E_{eq}), initial dynamic (E_o) and strain dependent dynamic (E_ε) moduli values obtained from the biomechanical testing and the biochemical parameters measured from the control and treated tissue groups ($n = 7$ per tissue group). Moduli values reported in MPa, water content reported as a percent (%), collagen reported in mg/mg dry weight, Pent, HP and LP reported in mmol/mol collagen. Mean values (±95% CI) are presented and statistical differences between the groups are denoted by the superscript letters. The *P*-values are generated from comparing each listed parameter between the two groups ($P < 0.05$ for significant differences)

Group	Biomechanical parameters (mean ± CI)			Biochemical parameters (mean ± CI)				
	E_{eq}	E_0	E_ε	Water	Collagen	Pent	HP	LP
Control	0.2 ± 0.0	1.6 ± 0.4	35.2 ± 6.3	80.2 ± 3.0	0.5 ± 0.2	0.4 ± 0.6	2649 ± 438	34.2 ± 7.8
Treated	0.4 ± 0.1	1.1 ± 0.7	48.4 ± 7.9	81.9 ± 4.2	0.6 ± 0.6	3.2 ± 1.3	2423 ± 385	36.8 ± 9.7
P-value	<0.001	0.189	0.008	0.452	0.860	<0.001	0.364	0.620

increase in cell volume change within the deep zone of the treated group (relative to the control group) was due to a ~5% and ~6% increase in cell expansion in both the width and depth directions (respectively).

Potential mechanisms involved in altering biomechanical cell responses due to ribose treatment

Several mechanisms may explain the altered biomechanical cell responses due to *in vitro* glycation. The smaller change in cell volumes and dimensions observed in the upper tissue zone of the treated group (relative to the control group) may be explained by the increase in Pent (Table I), carbohydrate content [Fig. 5(b), (e)] and/or elevated levels of fixed charge density [Fig. 5(d)]. These observed differences may indicate an increase in tissue cross-links and/or glycation[37] which may have led to increased tissue stiffness. Because local axial strains generate tensile forces in the tangentially oriented collagen fibrils in this zone[31,32], the generation of less local axial tissue strains in the treated tissues (region 1 in Fig. 4) may suggest that the collagen fibrils are 'pulling' the cells (possibly through integrin cell surface receptors anchored to the collagen network providing a pathway for force transmission to occur from the surrounding matrix to the cell[6,8]) less in the lateral direction. The reduced volume and lateral expansion of the upper zone cells simultaneously with the reduced local tissue strain from the treated group may also suggest that ribose treatment of AC mechanically stiffens the matrix surrounding the chondrocytes (through an increase in glycation), partially shielding them from deformation-induced cell volume and dimensional changes. These support the idea that the PCM, local collagen network and cross-

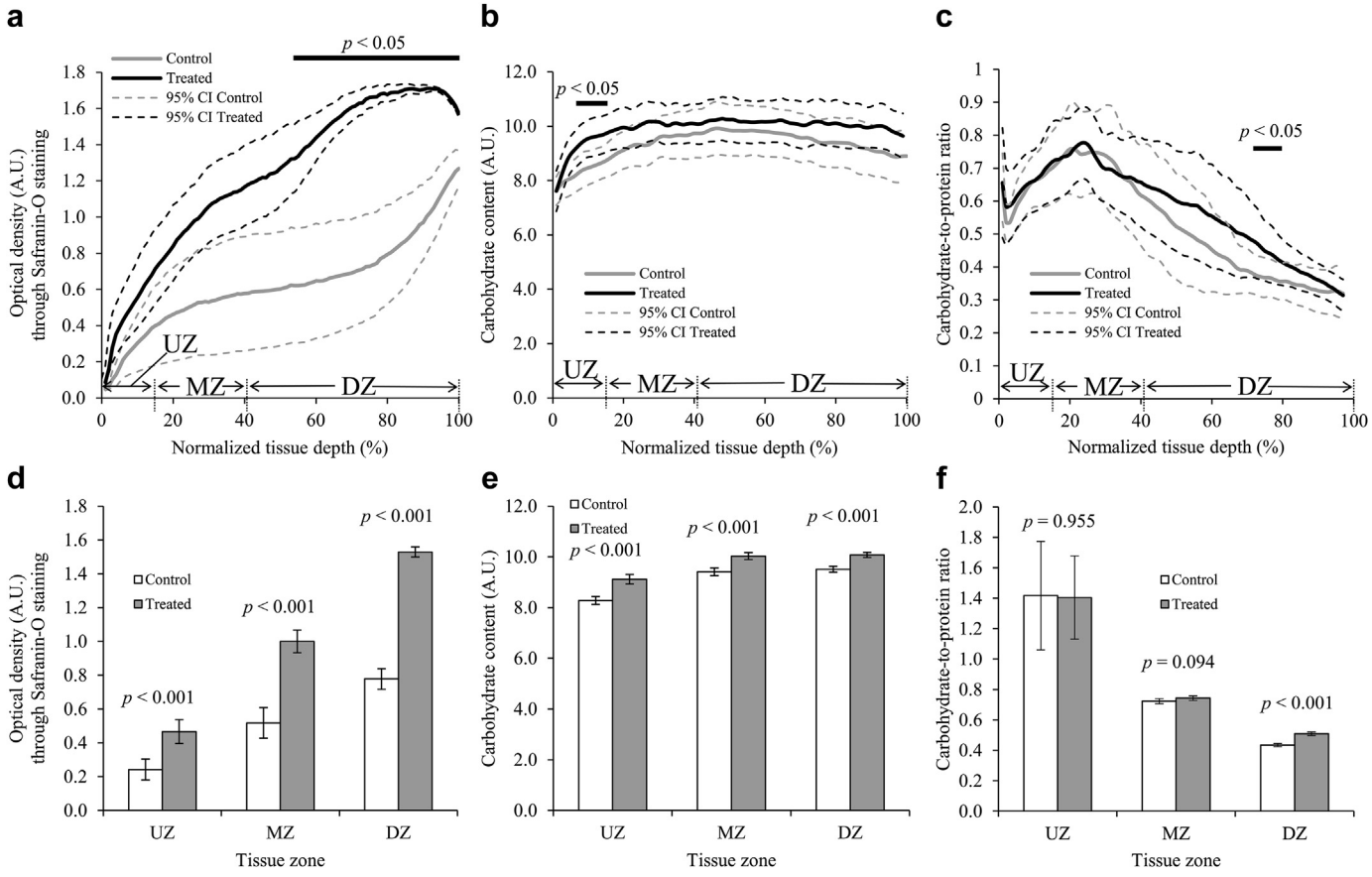

Fig. 5. Mean values (±95% CI) of the tissue properties plotted as a function of normalized tissue depth for the control and treated groups. a) optical density determined by DD[36]; b) carbohydrate content determined by FTIRI[37]; c) carbohydrate to protein ratio determined by FTIRI[37]. Mean values (±95% CI) determined for the zonal boundaries utilized for the cell deformation experiments. d) optical density; e) carbohydrate content; f) carbohydrate to protein ratio. A.U. = absorption unit; UZ, MZ and DZ correspond to the upper, middle and deep tissue zones, respectively. All data was obtained from three tissue sections per sample (seven samples per group). The solid black lines (above the graphs) denote statistical differences between groups ($P < 0.05$) in Fig. 5(a)–(c).

links (tissue glycation) may protect superficial zone cells from excessive strains and stresses[30–33,40]. These above mentioned superficial zone mechanisms may also explain the smaller observed cell shape changes (heights/depths) in the middle zone of the treated group.

The increase in Pent (Table I), fixed charge density [Fig. 5(a), (d)] and carbohydrate to protein ratio [Fig. 5(c), (f)] may provide an explanation for the deformation-induced increase in cell volumes in the deep zone. These observed differences may indicate an increase in tissue cross-links and/or glycated proteins, AGEs or precursors of AGEs in this zone[37] which may have led to an increase in fixed charge density. The fixed charge density is known to modify swelling pressure in cartilage. Thus, the increased osmotic pressure within the deeper zone [Fig. 5(a)] may have increased the tissue stiffness and also caused stiffening of the local collagen network in the ECM/PCM[13,28–30]. It may be that a stiffer ECM/PCM caused cells to become more compressed in the deep tissue which, in turn, caused elevated levels of lateral cell expansion. This is supported by the elevated levels of local axial strain in the deeper regions of the treated tissue suggesting that the mechanical signals were attenuated into greater tissue depths. Greater local strains in the deeper tissue may have caused collapsing of the vertical collagen fibrils which could have provided the cells greater space to elongate in the lateral direction. This is also supported by the elevated transverse strains (although not statistically significant) in the treated group (region 3 in Fig. 4). However, this could also be due to the stiffer tissue surrounding cells (due to the increased fixed charge density) 'pulling' deeper zone cells in the lateral direction. This speculation is anyhow consistent with earlier theoretical observations[31,32].

General characteristics of biomechanical and biochemical analyses

Ribose treatment utilized in this study had a clear effect on the elastic properties of AC, by increasing both the equilibrium modulus and the strain dependent dynamic modulus, while not significantly affecting the initial dynamic modulus of the tissue. These moduli changes due to the ribose treatment are also consistent with a previous study that utilized threose for *in vitro* glycation[21]. However, it should be noted that this was the first study where ribose was utilized to study biomechanical responses of live cells in aging cartilage and this treatment did not appear to alter cell viability (the green stained cells in Figs. 1(b), (c) and 3(a)). The relatively short period of time used in this current study and lower dosage of ribose (30 mM over 42 h of incubation) was selected in order to minimize cell death within the osteochondral explants, as live cells were required for imaging and the determination of chondrocyte biomechanical responses.

Previous studies have shown that HP and LP crosslinks are not correlated with age in human cartilage, whereas Pent cross-links are[11]. In this study, only increased levels of Pent were observed, consistent with previous studies utilizing ribose for *in vitro* cartilage glycation[11,14,15]. Although levels of Pent in human cartilage can only be used as an indication of the overall amount of collagen cross-links within the tissue, the elevated levels of Pent measured in the current study are consistent with aging in adult cartilage[11,13,15].

Significance of cross-linking in relation to aging and OA

In AC, AGE-induced changes in chondrocyte synthesis include decreased collagen turnover (i.e., decreasing both collagen synthesis and degradation)[17] and proteoglycan synthesis (a heavily glycosylated protein that provides compressive resistance in AC)[19]. However, these changes alone do not accelerate OA[20]. Although caution is warranted over the implications of our findings, AC aging may alter the mechanical signals that cells receive in the upper and deeper tissue zones. A change in the mechanical signals (i.e., either elevated or reduced levels) experienced by chondrocytes in AC may directly alter cellular biosynthesis and impair tissue health[41–46]. Researchers have shown the mechanobiological importance of abnormal mechanical conditions in AC and how they can elevate levels of metalloproteinase MMP-13 production (a proteolytic enzyme that is known to degrade collagen type II)[9,42,43,46] and suppress proteoglycan synthesis[41,43–45]. Thus, both the combined net effect of AGE accumulation and the abnormal mechanical loading conditions experienced by cells in AC may contribute to the long-term tissue changes rendering it susceptible to biomechanical dysfunction and OA. It is interesting to point out that tissue age is positively correlated with stiffening of the collagen network[11,13–15] and lower levels of tensile failure strain[47], making cartilage more brittle[11,13–15]. However in OA, degeneration-based changes such as collagen network destructuring[48] and proteoglycan loss[49] occur, causing tissue softening which may compensate for the effect of tissue stiffening associated with aging. Thus, over long-term time periods, depth-wise cell responses should also be affected by the net contribution from aging and OA.

Limitations

Though the current study provides new insight into the deformation response of chondrocytes in ribose treated tissue, there are limitations that must be considered. In order to induce cross-linking within the treated samples, approximately 42 h of incubation was performed on both tissue groups to allow for an appropriate comparison between them. However, any proteoglycan loss from the tissues is considered negligible as previous research demonstrated that even at 48 h of incubation there is negligible proteoglycan loss from AC[50]. Additionally, incubation with protease inhibitors to ensure minimal proteoglycan loss from these tissues was not possible as protease inhibitors have the potential to damage subchondral bone, thus potentially altering how cells in the osteochondral explants respond to deformation[51].

In order to capture the response of chondrocytes to deformation in the upper, middle and deep tissue zones, the cylindrical osteochondral plugs were cut in half and the cells were then imaged through the exposed cut tissue edge at a maximum focal depth of approximately 50 μm. This sample preparation could loosen the structure of the AC specimens which could affect the *in situ* response of chondrocytes to compression[26,27,30]. However, this is currently the only way to measure cells in a depth-dependent manner, since there are no techniques at the moment which could detect middle and deep zone cells through intact cartilage surfaces. Furthermore, both the treated and untreated cartilage samples underwent identical sample preparation steps so as to allow an appropriate comparison between the tissue groups.

Cross-linking markers such as Pent, HP, and LP[11] have been shown to vary depth-wise in AC. However, not all AGEs have been characterized in AC[15,25]. Thus, this makes determining zonal or depth-wise variation in these or other specific AGE-related markers challenging. In this current study the zonal variation of Pent, HP or LP was not investigated. This is because an analysis of this type would require sectioning AC into layers. This means that larger samples, larger than those we used here, would have probably been needed for a reliable HPLC analysis. Then obtaining tissue within the distal lateral quadrant of the patellae would have been very difficult to achieve, as the cylindrical samples harvested from the osteochondral plugs were already as large as the entire lateral quadrant of patella (Fig. 1). Because we originally wanted to compare the water content between tissue groups (in case ribose treatment was altering tissue water content), we decided that

sectioning samples into different layers would have altered this measurement. This would have likely altered the water content differently between the groups because stiffer ribose-treated samples would have likely experienced less loosening of the collagen fibril tension and subsequently less tissue swelling. This artifact of tissue swelling was also eliminated in our depth-wise microscopic and spectroscopic analyses where fully intact tissues attached to the subchondral bone were used. However, our FTIRI analysis has demonstrated depth-wise differences in tissue glycation that has been suggested to be indirectly related to AGEs or precursors of AGEs[37,39].

Conclusions

We investigated how *in vitro* glycation alters the deformation response of chondrocytes within mechanically compressed AC. Ribose treatment was found to decrease cell deformation responses in the upper tissue zone, transmit mechanical forces deeper into the tissue and increase cell deformation responses in the deeper tissue zone. These findings highlight the importance of how glycation, one of the signs of aging cartilage, can alter the biomechanical responses of chondrocytes in AC.

Contributions

JMF conceived the study with RKK and all authors were involved in the design of the experiments. JMF and MRH conducted confocal microscopy experiments. MRH performed the cell volume measurements, FTIRI measurements and both the PLM measurements and analysis. JMF performed pilot studies, sample preparation, cell dimensional measurements, biomechanical experiments, DD measurements and analyzed the obtained cell volume/dimensional, biomechanical, biochemical, DD and FTIRI measurements. All authors were involved in interpretation of the results. JMF wrote the first draft of the manuscript; all authors gave comments to and accepted the submitted manuscript.

Conflict of interests

None.

Acknowledgments

The authors would like to thank funding provided by the European Research Council under the European Union's Seventh Framework Programme (FP/2007–2013)/ERC Grant Agreement no. 281180, Academy of Finland (projects 140730 and 218038), Finnish Cultural Foundation Post-Doctoral Research Grant, Orion-Farmos Research Foundation, Magnus Ehrnrooth Foundation, Sigrid Juselius Foundation and the Kuopio University Hospital (Department of Clinical Physiology and Nuclear Medicine, EVO). The Department of Anatomy at the University of Eastern Finland (Dr Kirsi Rilla and Mr Kari Törrönen) is acknowledged for their technical assistance and Dr Vuokko Kovanen (Department of Health Sciences, University of Jyväskylä, Jyväskylä, Finland) is also acknowledged for providing us with the biochemical measurements from our tissue groups. Jukka Laakkonen is acknowledged for designing the microcompression device.

Supplementary data

Supplementary data related to this article can be found at http://dx.doi.org/10.1016/j.joca.2014.07.020.

References

1. CDC. Prevalence of doctor-diagnosed arthritis and arthritis-attributable activity limitation-United States, 2010–2012. MMWR Morb Mortal Wkly Rep 2013;62:869–73.
2. Lawrence RC, Felson DT, Helmick CG, Arnold LM, Choi H, Deyo RA, *et al*. Estimates of the prevalence of arthritis and other rheumatic conditions in the United States: Part II. Arthritis Rheum 2008;58:26–35.
3. Li YP, Wei XC, Zhou JM, Wei L. The age-related changes in cartilage and osteoarthritis. Biomed Res Int 2013;2013:1–12. Article ID 916530.
4. Verzijl N, Bank RA, TeKoppele JM, DeGroot J. AGEing and osteoarthritis: a different perspective. Curr Opin Rheumatol 2003;15:616–22.
5. Lotz M, Loeser RF. Effects of aging on articular cartilage homeostasis. Bone 2012;51:241–8.
6. Wilkins RJ, Browning JA, Urban JPG. Chondrocyte regulation by mechanical load. Biorehology 2000;37:67–74.
7. Hügle T, Geurts J, Nüesch C, Müller-Gerbl M, Valderrabano. Aging and osteoarthritis: an inevitable encounter? J Aging Res 2012:1–7. Article ID 950192.
8. Bader DL, Salter DM, Chowdhury TT. Biomechanical influence of cartilage homeostasis in health and disease. Arthritis 2011: 1–16. Article ID 979032.
9. Sun HB. Mechanical loading, cartilage degradation, and arthritis. Ann N Y Acad Sci 2009;2011:37–50.
10. Eyre DR, Dickson IR, Van Ness K. Collagen cross-linking in human bone and articular cartilage. Age-related changes in the content of mature hydroxypyridinium residues. Biochem J 1988;252:495–500.
11. Bank RA, Bayliss MT, Lafeber JG, Maroudas A, TeKoppele JM. Ageing and zonal variation in post-translational modification of collagen in normal human articular cartilage. The age-related increase in non-enzymatic glycation affects biomechanical properties of cartilage. Biochem J 1998;330: 345–51.
12. Verzijl N, DeGroot J, Thorpe SR, Bank RA, Shaw JN, Lyons TJ, *et al*. Effect of collagen turnover on the accumulation of advanced glycation end products. J Biol Chem 2000;275: 39027–31.
13. Verzijl N, DeGroot J, Ben ZC, Brau-Benjamin O, Maroudas A, Bank RA, *et al*. Crosslinking by advanced glycation end products increases the stiffness of the collagen network in human articular cartilage: a possible mechanism through which age is a risk factor for osteoarthritis. Arthritis Rheum 2002;46: 114–23.
14. Chen AC, Temple MM, Ng DM, Verzijl N, Degroot J, TeKoppele JM, *et al*. Induction of advanced glycation end products and alterations of the tensile properties of articular cartilage. Arthritis Rheum 2002;46:3212–7.
15. Verzijl N, DeGroot J, Oldehinkel E, Bank RA, Thorpe SR, Baynes JW, *et al*. Age-related accumulation of millard reaction products in human articular cartilage. J Biol Chem 2000;275: 39027–31.
16. Chahine NO, Blanchette C, Thomas CB, Lu J, Haudenschild D, Loots GG. Effect of age and cytoskeletal elements on the indentation-dependent mechanical properties of chondrocytes. PLoS One 2013;8:e61651. 1–11.
17. Duan W-P, Sun Z-W, Li Q, Li C-J, Wang L, Chen W-Y, *et al*. Normal age-related viscoelastic properties of chondrons and chondrocytes isolated from rabbit knee. Chin Med J (Engl) 2012;125:2574–81.
18. DeGroot J, Verzijl N, Budde M, Bijlsma JW, Lafeber FP, TeKoppele JM. Accumulation of advanced glycation end

products decreases collagen turnover by bovine chondrocytes. Exp Cell Res 2001;266:303–10.
19. DeGroot J, Verzijl N, Bank RA, Lafeber FP, Bijlsma JW, TeKoppele JM. AGE-related decrease in proteoglycan synthesis of human articular cartilage: the role of nonenzymatic glycation. Arthritis Rheum 1999;42:1003–9.
20. Vos PAJM, DeGroot J, Barten-van Rijbroek AD, Zuurmond A-M, Bijlsma JWJ, Mastbergen SC, *et al*. Elevation of cartilage AGEs does not accelerate initiation of canine experimental osteoarthritis upon mild surgical damage. J Orthop Res 2012;30:1398–404.
21. Kokkonen HT, Mäkelä J, Kulmala KAM, Rieppo L, Jurevelin JS, Tiitu V, *et al*. Computed tomography detects changes in contrast agent diffusion after collagen cross-linking typical to natural aging of articular cartilage. Osteoarthritis Cartilage 2011;19:1190–8.
22. Willett TL, Kandel R, De Croos JNA, Avery NC, Grynpas MD. Enhance levels of non-enzymatic glycation and pentosidine crosslinking in spontaneous osteoarthritis progression. Osteoarthritis Cartilage 2012;20:736–44.
23. Valencia JV, Weldon SC, Quinn D, Kiers GH, DeGroot J, TeKoppele JM, *et al*. Advanced glycation end product ligands for the receptor for advanced glycation end products: biochemical characterization and formation kinetics. Anal Biochem 2004;324:68–78.
24. Bailey AJ, Sims TJ, Avery NC, Halligan EP. Non-enzymic glycation of fibrous collagen: reaction products of glucose and ribose. Biochem J 1995;305:385–90.
25. Paul RG, Avery NC, Slatter DA, Sims TJ, Bailey AJ. Isolation and characterization of advanced glycation end products derived from the in vitro reaction of ribose and collagen. Biochem J 1998;320:1241–8.
26. Guilak F, Ratcliffe A, Mow VC. Chondrocyte deformation and local tissue strain in articular cartilage: a confocal microscopy study. J Orthop Res 1995;13:410–21.
27. Youn I, Choi JB, Cao L, Setton LA, Guilak F. Zonal variations in the three dimensional morphology of the chondron measured in situ using confocal microscopy. Osteoarthritis Cartilage 2006;14:889–97.
28. Han S-K, Seerattan R, Herzog W. Mechanical loading of in situ chondrocytes in lapine retropatellar cartilage after anterior cruciate ligament transection. J R Soc Interface 2010;7:895–903.
29. Turunen SM, Han S-K, Herzog W, Korhonen RK. Cell deformation behavior in mechanically loaded rabbit articular cartilage 4 weeks after anterior cruciate ligament transaction. Osteoarthritis Cartilage 2013;21:505–13.
30. Madden R, Han S-K, Herzog W. Chondrocyte deformation under extreme tissue strain in two regions of the rabbit knee joint. J Biomech 2013;46:554–60.
31. Korhonen RK, Herzog W. Depth-dependent analysis of the role of collagen fibrils, fixed charges and fluid in the pericellular matrix of articular cartilage on chondrocyte mechanics. J Biomech 2008;41:480–5.
32. Korhonen RK, Julkunen P, Wilson W, Herzog W. Importance of collagen orientation and depth-dependent fixed charge densities of cartilage on mechanical behavior of chondrocytes. J Biomech Eng 2008;130:021003.
33. Tanska P, Turunen SM, Han SK, Julkunen P, Herzog W, Korhonen RK. Superficial collagen fibril modulus and pericellular fixed charge density modulate chondrocyte volumetric behaviour in early osteoarthritis. Comput Math Methods Med 2013;2013. Article ID 164146.
34. Mow VC, Guo XE. Mechano-electricalchemical properties of articular cartilage: their inhomogeneties and anisotropies. Annu Rev Biomed Eng 2002;4:175–2009.
35. Bush PG, Hall AC. Regulatory volume decrease (RVD) by isolated and in situ bovine articular chondrocytes. J Cell Physiol 2001;187:304–14.
36. Kiviranta I, Jurvelin J, Tammi M, Säämänen AM, Helminen HJ. Microspectrophotometric quantitation of glycosaminoglycans in articular cartilage sections stained with Safranin O. Histochemistry 1985;82:249–55.
37. Birarda G, Holman EA, Fu S, Weikel K, Hu P, Blankenberg FG, *et al*. Synchrotron infrared imaging of advanced glycation endproducts (AGEs) in cardiac tissue from mice fed high glycemic diets. Biomed Spectrosc Imaging 2013;2:301–15.
38. Király K, Hyttinen MM, Lapveteläinen T, Elo M, Kiviranta I, Dobai J, *et al*. Specimen preparation and quantification of collagen birefringence in unstained sections of articular cartilage using image analysis and polarizing light microscopy. Histochem J 1997;29:317–27.
39. Guilbert M, Said G, Happillon T, Untereiner V, Garnotel R, Jeannesson P, *et al*. Probing non-enzymatic glycation of type I collagen: a novel approach using Raman and infrared biophotonic methods. Biochim Biophys Acta 2013;1830:3525–31.
40. Guilak F, Alexopoulos LG, Upton ML, Youn I, Choi JB, Cao L, *et al*. The pericellular matrix as a transducer of biomechanical and biochemical signals of articular cartilage. Ann N Y Acad Sci 2006;1068:498–512.
41. Martin JA, Brown T, Heiner A, Buckwalter JA. Post-traumatic osteoarthritis: the role of accelerated chondrocyte senescence. Biorheology 2004;41:479–91.
42. Pirttiniemi P, Kantomaa T, Sorsa T. Effect of decreased loading on the metabolic activity of the mandibular condylar cartilage in rat. Eur J Orthod 2004;26:1–5.
43. Beckett J, Jin W, Schultz M, Chen A, Tolbert D, Moed BR, *et al*. Excessive running induces cartilage degeneration in knee joints and alters gait of rats. J Orthop Res 2012;30:1604–10.
44. Roemhildt ML, Beynnon BD, Gauthier AE, Gardner-Morse M, Ertem F, Badger GJ. Chronic in vivo load alteration induces degenerative changes in the rat tibiofemoral joint. Osteoarthritis Cartilage 2013;21:346–57.
45. Jorktikka MO, Inkinen RI, Tammi MI, Parkkinen JJ, Haapala J, Kiviranta I, *et al*. Immobilisation causes longlasting matrix changes both in the immobilized and contralateral joint cartilage. Ann Rheum Dis 1997;56:255–61.
46. Wu W, Billinghurst C, Pidoux I, Antoniou J, Zukor D, Tanzer M, *et al*. Sites of collagenase cleavage and denaturation of type II collagen in aging and osteoarthritic articular cartilage and their relationship to the distribution of matrix metalloproteinase 1 and matrix metalloproteinase 13. Arthritis Rheum 2002;46:2087–94.
47. Kempson GE. Relationship between the tensile properties of articular cartilage from the human knee and age. Ann Rheum Dis 1982;41:508–11.
48. Buckwalter JA, Mankin HJ, Grodzinsky AJ. Articular cartilage and osteoarthritis. Instr Course Lect 2005;54:465–80.
49. Malemud CJ. Changes in proteoglycans in osteoarthritis; biochemistry, ultrastructure and biosynthetic processing. J Rheumatol Suppl 1991;27:60–2.
50. Huttu M, Turunen S, Sokolinski V, Tiitu V, Lammi M, Korhonen RK. Effects of medium and temperature on cellular responses in the superficial zone of hypo-osmotically challenged articular cartilage. J Funct Biomater 2012;3:544–55.
51. Willett TL, Whiteside R, Wild PM, Wyss PM, Anastassiades T. Artefacts in the mechanical characterization of porcine articular cartilage due to freezing. Proc Inst Mech Eng H 2005;219:23–9.